Available online at www.sciencedirect.com
SCIENCE DIRECT®
PERGAMON
International Journal of Heat and Mass Transfer 46 (2003) 2039–2049
International Journal of HEAT and MASS TRANSFER
www.elsevier.com/locate/ijhmt

Effect of mixed convection on transient hydrodynamic removal of a contaminant from a cavity

Lih-Chuan Fang *

Department of Mechanical Engineering, Chinese Military Academy, P.O. Box 90602-6, Fengshan, Kaohsiung 830, Taiwan, ROC

Received 17 July 2002; received in revised form 11 October 2002

Abstract

A preliminary numerical study of the effect of mixed convection on hydrodynamic removal of contaminants contained in a cavity is carried out. The process of fluid renewal in a cavity is modeled via a numerical solution of the Navier–Stokes equations coupled with the energy equation for transient flows. Attention in the present work is focused on the effects of mixed convection on the transient development of a cavity flow and the efficiency of cleaning cavities. The results show that the change in Grashof number causes a dramatic difference in the observed flow pattern and cleaning efficiency.

1. Introduction

The residues of industrial manufacturing processes can give rise to an accumulation of deposits in cavities of rough surfaces and those which may arise through poorly fitted components and junctions in the pipe work. The quality and cleanliness of the processed material is maintained by periodically cleaning the ducts and pipelines. In recent years, hydrodynamic cleaning of components, parts and pipelines has become widely accepted, since solvents used to clean a system can be environmentally harmful. However there are many problems which involve distinct cavities in the pipelines and the cleaning of these can lead to quite difficult problems. Due to the presence of recirculating vortices in cavities of rough surfaces, it is found to be difficult to remove all traces of residues. Consequently the modeling of duct flow over a cavity is considered as a starting point for assessing the effect of a flow in removing material initially contained in a cavity.

Numerous studies of duct flow over cavities have been reported in the past few decades. The previous results [1–3] showed that the separation streamline and the intensity of the closed streamline flow within the cavity are a function of cavity aspect ratio, relative duct size to cavity size, and the parallel velocity within the duct. These important recirculation regions may be observed in the problem of cavity cleaning. In addition, studies of mass transfer in a cavity have appeared in the pertinent literature [4–8]. However, most previous studies have assumed that the velocity components in the cavity are those which exist in steady state conditions. Recently, Fang et al. [9] have presented a numerical and experimental study of the time-dependent hydrodynamic removal of a contaminated fluid from a cavity on the floor of a duct. It was shown that the cleaning of the foulant with the same density as the fluid in the duct is more pronounced during the unsteady start-up of the duct flow and the rate of cleaning decreases as the flow reaches a steady state. The cleaning process is enhanced as the cavity aspect ratio (width/depth) is increased and as the duct Reynolds number increases.

The applications of convective heat transfer problems are numerous in the chemical and food processing industry. Relatively few studies, however, deal with the problem of hydrodynamic removal under the effect of convective heat transfer. Hence, the extension to such problem is important in hydrodynamic cleaning. In recent years, the study of convective heat transfer in a

* Tel.: +886-7-7466641; fax: +886-7-7104697.
E-mail address: lcfang@cc.cma.edu.tw (L.-C. Fang).

0017-9310/03/$ - see front matter © 2003 Elsevier Science Ltd. All rights reserved.
doi:10.1016/S0017-9310(02)00507-0

Nomenclature

AR	cavity aspect ratio (Width/Depth)
D	cavity depth
$D_{i,k}^{n+1}$	indication of finite difference form of the continuity equation
Gr	Grashof number $(= g\beta\Delta TH^3/v^2)$
g	gravitational acceleration
H	duct height
Pr	Prandtl number $(= v/\alpha)$
p	pressure
q_s	heat source
Re	Reynolds number $(= UH\rho/\mu)$
R_f	relaxation parameter
T	temperature
T_i	inflow temperature
t	time variable
U	maximum velocity of duct flow
u	velocity in the horizontal direction
W	cavity width
w	velocity in the vertical direction
x	horizontal coordinate
z	vertical coordinate

Greek symbols

α	thermal diffusivity
β	coefficient of thermal expansion
ΔT	temperature scale $(= q_s H/k)$
δt	a time step
δx	length of a cell in x direction
δz	length of a cell in z direction
ε_D	convergence tolerance
η	indication of finite differencing form of Navier–Stokes equation
θ	dimensionless temperature $[= (T - T_i)/\Delta T]$
λ	a combination factor
μ	viscosity
v	kinematic viscosity
ρ	density

Subscripts

i	x direction index
k	z direction index

Superscripts

m	an iteration count
n	time level

cavity has increased. The previous studies [10–14] showed that the increase in the heat transfer rate is more rapid and the cavity flow patterns dramatically change, especially when natural convection is the dominant mode of heat transfer. For a cavity containing a contaminated fluid, the interaction between the external flow and the buoyancy driven flow generated by the heat source leads to the possibility of complex flows. From a mass transfer perspective, the renewal rate of a cavity fluid may be enhanced due to the buoyancy driven flow. Consequently it is of particular interest to know the effect of mixed convection in the hydrodynamic cleaning of a cavity.

The main purpose of the present study is to investigate the effect of mixed convection on hydrodynamic removal of contaminants from a cavity. Although for the higher renewal rate of the cavities the duct flow may be characterized by a turbulent regime, the present study is limited to the laminar regime as a first step. This work still covers a wide range of Grashof numbers, Reynolds numbers and cavity aspect ratios with respect to the cleaning rate in laminar regime. The process of fluid renewal in a cavity is modeled via a numerical solution of the Navier–Stokes equations coupled with the energy equation for transient flows. The numerical method used is based on the MAC (Marker and Cell) method of Harlow and Welch [15]. Passive markers are used to visualize the flow and to quantify the hydrodynamic cleaning of the cavities.

2. Physical model and numerical method

The geometry of the duct-cavity configuration employed in this study is shown in Fig. 1. A Cartesian coordinate system is used with origin at the lower left hand corner of the computational domain. The cavity dimensions are defined by width W and depth D. Fluid of density ρ and viscosity μ flows continuously into the duct from the left and exits on the right. The acceleration, due to gravity g, acts in the negative z-direction. The properties of the contaminated cavity fluid are as-

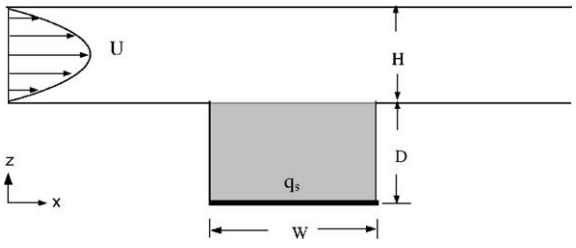

Fig. 1. A sketch of the co-ordinate system in a duct with a rectangular cavity.

sumed to be the same as for the fluid flowing in the duct. There is a constant-flux heat source q_s on the bottom wall of the cavity. All solid boundaries are assumed to be rigid no-slip walls. The height of the duct H was kept constant. Preliminary numerical experiments in the present study have indicated that entry lengths of twice the duct heights ($2H$) or greater cause negligible changes in the results. Entry lengths of $2H$ have been used for all the solutions presented in this study.

To non-dimensionalize the governing equations and the boundary conditions, the duct height H is chosen as the characteristic length, the maximum velocity of duct flow U as the characteristic velocity, the quantity ρU^2 as the characteristic pressure, and $q_s H/k$ as the characteristic temperature. The fundamental non-dimensional equations in Cartesian form for two-dimensional incompressible flow of a Newtonian fluid with constant properties are:

$$\frac{\partial u}{\partial x}+\frac{\partial w}{\partial z}=0 \tag{1}$$

$$\frac{\partial u}{\partial t}+\frac{\partial u^2}{\partial x}+\frac{\partial uw}{\partial z}=-\frac{\partial p}{\partial x}+\frac{1}{Re}\left(\frac{\partial^2 u}{\partial x^2}+\frac{\partial^2 u}{\partial z^2}\right) \tag{2}$$

$$\frac{\partial w}{\partial t}+\frac{\partial wu}{\partial x}+\frac{\partial w^2}{\partial z}=-\frac{\partial p}{\partial z}+\frac{1}{Re}\left(\frac{\partial^2 w}{\partial x^2}+\frac{\partial^2 w}{\partial z^2}\right)+\frac{Gr}{Re^2}\theta \tag{3}$$

$$\frac{\partial \theta}{\partial t}+\frac{\partial u\theta}{\partial x}+\frac{\partial w\theta}{\partial z}=\frac{1}{Re\cdot Pr}\left(\frac{\partial^2 \theta}{\partial x^2}+\frac{\partial^2 \theta}{\partial z^2}\right) \tag{4}$$

Where $Re = UH\rho/\mu$ is the Reynolds number, $Gr = g\beta\Delta TH^3/v^2$ is Grashof number and $Pr = v/\alpha$ is Prandtl number.

The flow field is discretized into cells of size $\delta x \times \delta z$ with cell centres being designated by indices i in the x direction and k in the z direction. The u values are located on the vertical sides of the cell, and w values on the horizontal upper and lower sides. The values of p and θ are located at the cell centres. The Navier–Stokes equations and energy equation are represented in a finite-difference form by forward differencing in time and centred differencing in space, except for the convection terms in the Navier–Stokes equations, where a combination of centred and upstream differencing is used. For example, if integer 'n' represents the time level, then u at a new $(n+1)$ time level is calculated from

$$(\rho u)^{n+1}_{i+1/2,k}=\eta_{i+1/2,k}-\frac{\delta t}{\delta x}\left(p^{n+1}_{i+1,k}-p^{n+1}_{i,k}\right) \tag{5}$$

where

$$\begin{aligned}\eta_{i+1/2,k}=(\rho u)_{i+1/2,k}&-\delta t(UXX_{i+1/2,k}+UXZ_{i+1/2,k})\\&+\frac{\delta t}{\delta x^2}Re^{-1}(u_{i+3/2,k}-2u_{i+1/2,k}+u_{i-1/2,k})\\&+\frac{\delta t}{\delta z^2}Re^{-1}(u_{i+1/2,k+1}-2u_{i+1/2,k}+u_{i+1/2,k-1})\end{aligned}$$

The convection terms in (5) are given by

$$\begin{aligned}UXX_{i+1/2,k}=\frac{1}{4\delta x}\Big\{&\left(u_{i+3/2,k}+u_{i+1/2,k}\right)^2-\lambda\left|u_{i+3/2,k}+u_{i+1/2,k}\right|\\&\times\left(u_{i+3/2,k}-u_{i+1/2,k}\right)-\left(u_{i+1/2,k}+u_{i-1/2,k}\right)^2\\&+\lambda\left|u_{i+1/2,k}+u_{i-1/2,k}\right|\left(u_{i+1/2,k}-u_{i-1/2,k}\right)\Big\}\end{aligned}$$

$$\begin{aligned}UXZ_{i+1/2,k}=\frac{1}{4\delta z}\Big\{&\left(w_{i,k+1/2}+w_{i+1,k+1/2}\right)\left(u_{i+1/2,k}+u_{i+1/2,k+1}\right)\\&-\lambda\left|w_{i,k+1/2}+w_{i+1,k+1/2}\right|\left(u_{i+1/2,k+1}-u_{i+1/2,k}\right)\\&-\left(w_{i+1,k-1/2}+w_{i,k-1/2}\right)\left(u_{i+1/2,k-1}+u_{i+1/2,k}\right)\\&+\lambda\left|w_{i,k-1/2}+w_{i+1,k-1/2}\right|\left(u_{i+1/2,k}-u_{i+1/2,k-1}\right)\Big\}\end{aligned}$$

where λ is a combination factor; $\lambda=0$ gives centred differencing and $\lambda=1$ gives upstream differencing. Approximate stability conditions for the iteration procedure are given by Miyata and Nishimura [16]:

$$\left(\frac{\delta t}{\delta x}u+\frac{\delta t}{\delta z}w\right)\leqslant\lambda\leqslant 1 \tag{6}$$

and

$$v\leqslant\frac{1-\lambda\left(\frac{\delta t}{\delta x}u+\frac{\delta t}{\delta z}w\right)}{2\delta t(1/\delta x^2+1/\delta z^2)} \tag{7}$$

Eq. (6) gives conditions for the combination factor and the Courant number, and it limits the distance a fluid particle can travel in one time step to the smallest side of a cell. Eq. (7) represents an upper limit on viscosity and it is important when highly viscous flows are being considered. A value of 0.5 is normally used to avoid instabilities arising from numerically introduced negative diffusion.

The solution is approached through the artificial compressibility method of Chorin [17] which involves a simultaneous iteration on pressure and velocity component. If $D^{n+1}_{i,k}$ represents the divergence of the fluid in a cell, where

$$D^{n+1}_{i,k}=\frac{1}{\delta x}\left(u^{n+1}_{i+1/2,k}-u^{n+1}_{i-1/2,k}\right)+\frac{1}{\delta z}\left(w^{n+1}_{i,k+1/2}-w^{n+1}_{i,k-1/2}\right) \tag{8}$$

then the pressure in cell i, k is updated through

$$\left(p^{n+1}_{i,k}\right)^{m+1}=\left(p^{n+1}_{i,k}\right)^{m}-R_f\left(D^{n+1}_{i,k}\right)^{m}$$

where m indicates the mth iteration and R_f is a relaxation parameter. The solution is reached when the magnitude of $D^{n+1}_{i,k}$ in each cell is less than some pre-set small value, typically $O(10^{-6})$. The stability restriction is given by $R_f\leqslant\rho\delta x^2/2\delta t$ [18]. The optimum value of R_f giving the most rapid convergence can, in general, only be determined by experimentation. $R_f=1.85$ is used in the present calculation.

In the original MAC method, the energy equation is solved by a time marching explicit method. Kuo et al.

[19] have reported that an explicit method may lead to non-physical results in the transient solution. Thus an implicit method is used to solve the energy equation in the present study. Therefore there are two iterative processes in each time step used to evaluate the pressure and velocity as well as temperature.

The computational mesh is surrounded by a one-cell-thick layer of cells, which are used for setting boundary conditions. No-slip boundary conditions are applied at all solid boundaries, a flow velocity is prescribed at the inflow boundary and zero normal gradients are used to set variables just outside the outflow boundary. The boundary conditions for the temperature is $\theta = 0$ at the inflow boundary. The insulated conditions are imposed at the wall and at outflow as well, while $\partial\theta/\partial z = -1$ is specified at the bottom of the cavity.

Flow visualization and fluid contamination calculations are made possible by the use of passive markers. These are initially distributed before start-up and are moved to new positions at each time step. The motion of each marker was recorded as the duct flow interacted with that in the cavity. The use of marker particles achieves the same effect as adding a diffusion equation in

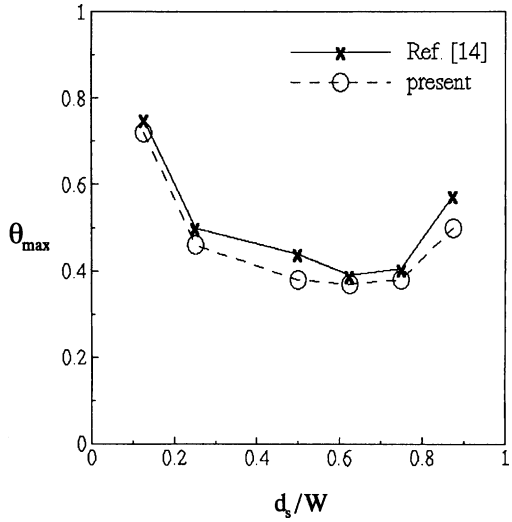

Fig. 2. Comparison of the results obtained using the present code with those of Papanicolaou and Jaluria [14] for $Re = 100$ and $Gr = 10000$. (d_s horizontal distance from the left vertical wall of the enclosure, W width of the enclosure).

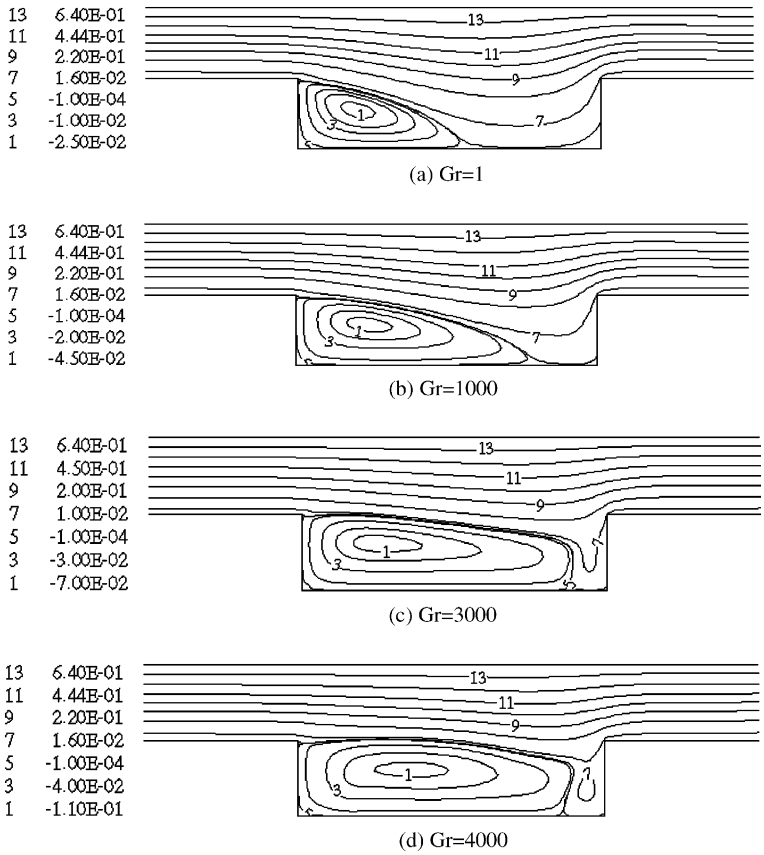

Fig. 3. Streamlines of duct flow over cavities with varied Grashof numbers, AR = 4 and $Re = 50$ at steady state.

which the diffusivity is taken as zero, and therefore the movement of the markers is entirely due to convection. For example the new x-position of a marker k at time level $n+1$ is calculated from $x_k^{n+1} = x_k^n + u_k^{n+1}\delta t$ where u_k is the horizontal velocity at the marker position, x_k^n. The velocity components at the marker positions are calculated by a weighted interpolation of velocities in surrounding cells as described by Welch et al. [20].

The computer code has been validated by application to the problem for which solutions are available. The test was with mixed convection from an isolated heat source in a rectangular enclosure when $Re = 100$ and $Gr = 10000$ as considered by Papanicolaou and Jaluria [14]. The good agreement shown in Fig. 2 was obtained by comparing maximum source temperature θ_{max} for various source locations from the present method with those from Papanicolaou and Jaluria [14].

3. Results and discussion

The present investigation covers a range of Grashof numbers, $Gr = 1 - 4000$, cavity aspect ratios (Width/Depth), $AR = 0.25 - 4$, and Reynolds numbers, $Re = 50 - 1600$. A Prandtl number of water was assumed, $Pr = 7$. The flow is always considered to be laminar and the foulant has the same density as the fluid in the duct. In addition, the duct velocity profile is considered to be Poiseuille flow.

Fig. 3 shows the streamlines for $Gr = 1 - 4000$ while keeping $Re = 50$ and $AR = 4.0$. For $Gr = 1$, the flow penetration to the bottom of the cavity remains eventually one large main vortex in the upstream corner of the cavity, similar to the results without the effect of mixed convection by Fang et al. [9]. As the Grashof number is increased, different flow patterns are encountered due to stronger buoyancy effect. It can be seen that the area of the main vortex in the cavity is increased with the increase of Gr. For Gr larger than 3000, the main vortex occupied a large portion of the cavity. It is worth mentioning that for the values of Gr higher than 4000 the steady state result could not be obtained, since oscillatory behavior was observed. At such large value, small disturbances in the flow can give rise to a transition to turbulent flow. Thus, $Gr = 4000$ is selected as the maximum Grashof number in the present study. The

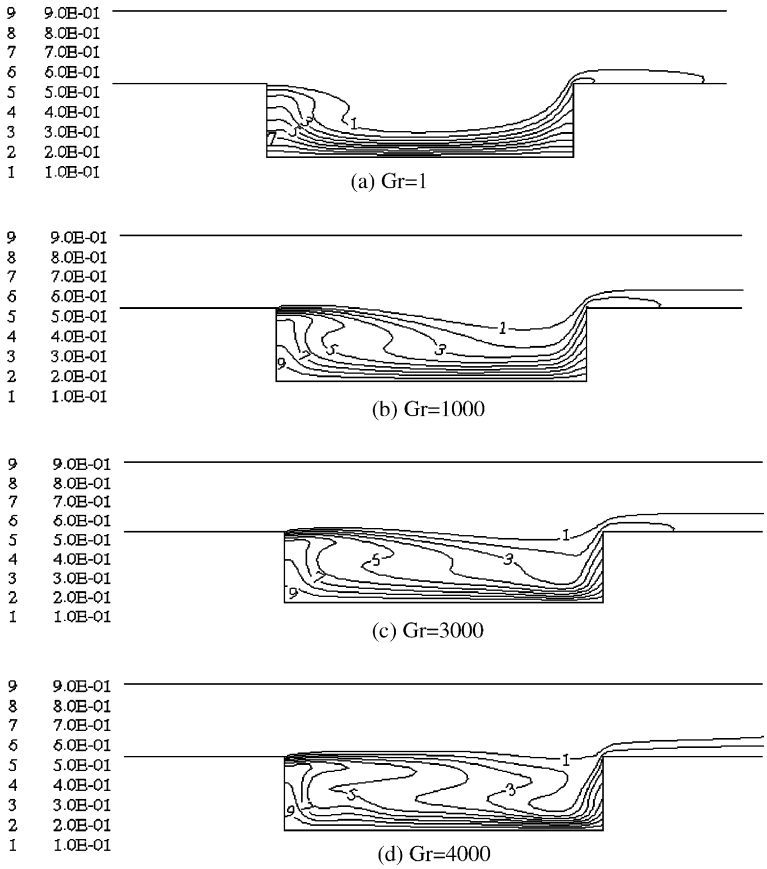

Fig. 4. Isotherms of duct flow over cavities with varied Grashof numbers, $AR = 4$, and $Re = 50$ at steady state.

corresponding isotherms varied with Grashof number are shown in Fig. 4. For low Grashof number $Gr = 1$, the isotherm shows that a large area of the cavity remains at low temperature. For large values of Gr, most of the area of the cavity remains at the high temperature due to stronger buoyancy. Clearly, the greater Grashof number causes stronger recirculation and enhances heat transfer in the cavity as well.

Streamlines and isotherms, for two cavities of aspect ratios AR = 1 and 0.25, with $Gr = 1000$ and 4000 respectively, are shown in Figs. 5 and 6. For AR = 1 and $Gr = 1000$, the main vortex fills the cavity. As $Gr = 4000$, different flow pattern in the cavity appears. There is a pair of counter-rotating vortices in the cavity shown in Fig. 5(a). It can be seen from Fig. 5(b) that the heat transfer in the cavity is enhanced with the increase of Gr. For a deeper cavity with AR = 0.25, Fig. 6(a) shows three sub-regions formed finally and one small isolated vortex in the corner as $Gr = 1000$. This is analogous to the situation documented for the deep cavities. It is observed that the strength of circulation is stronger for $Gr = 4000$ and the small corner vortex grows. In addition, the stronger buoyancy enhances the heat transfer in the cavity as illustrated in Fig. 6(b).

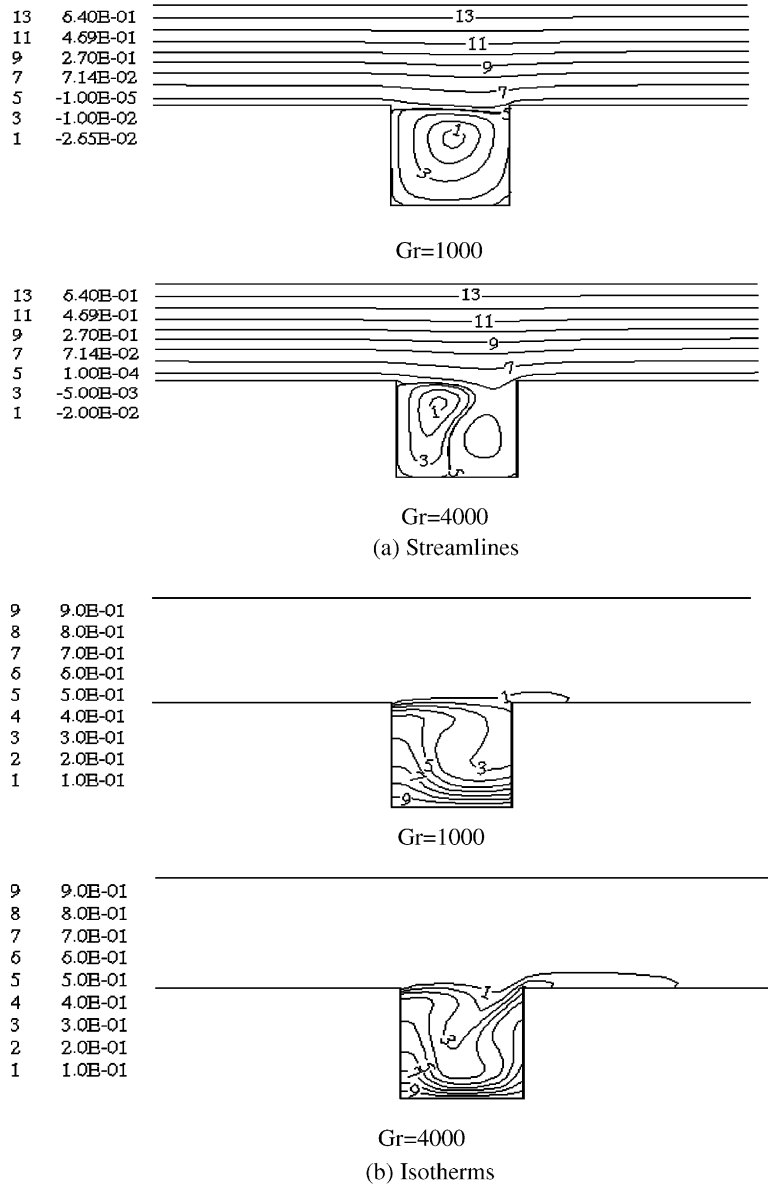

Fig. 5. (a) Streamlines and (b) isotherms of duct flow over cavities with varied Grashof numbers, AR = 1 and $Re = 50$ at steady state.

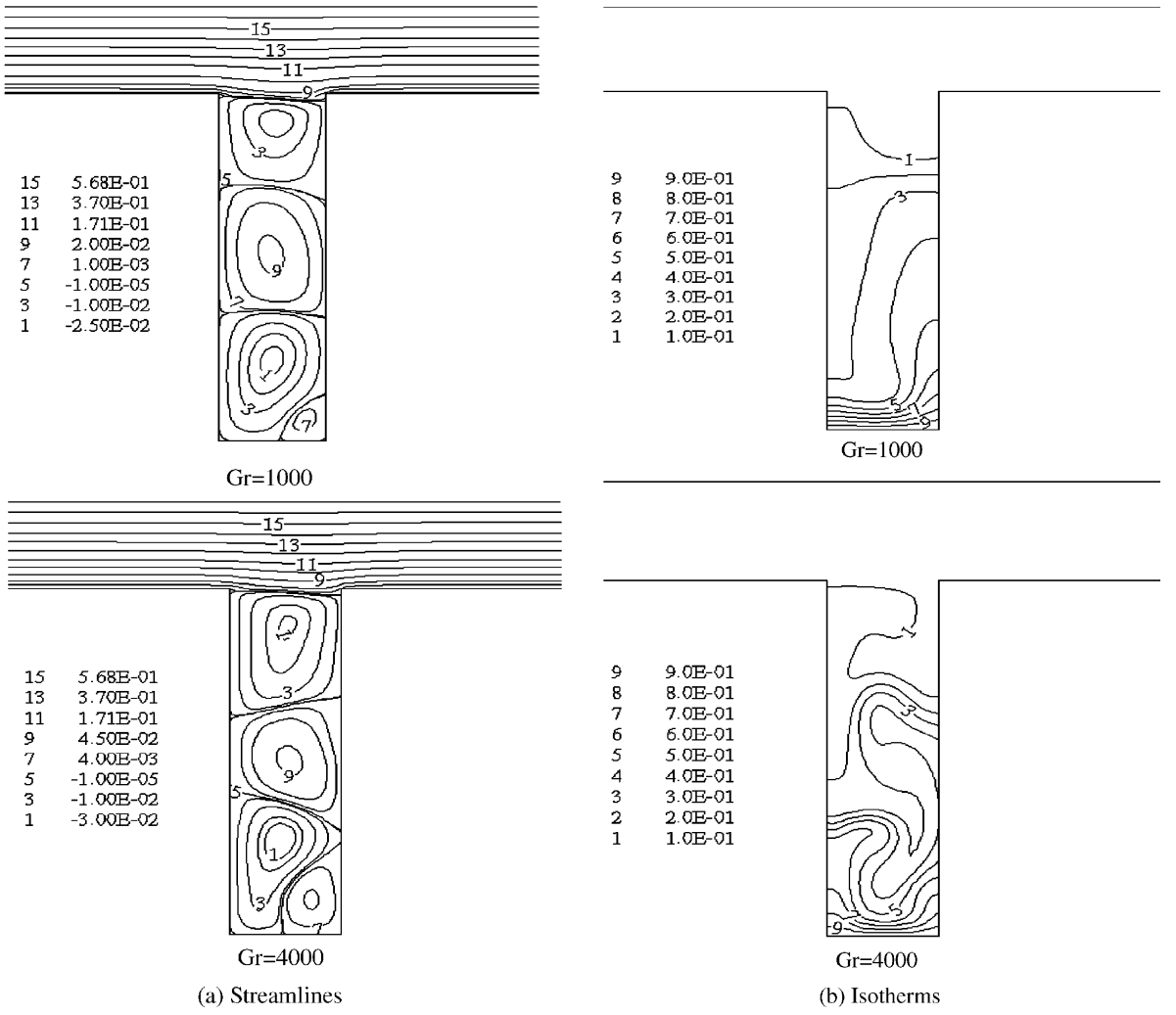

Fig. 6. (a) Streamlines and (b) isotherms of duct flow over cavities with varied Grashof numbers, AR = 0.25 and $Re = 50$ at steady state.

By measuring the area covered by the recirculating fluid in the cavity it is possible to estimate the fraction of a cavity area that will contain contaminated fluid soon after a steady state is reached; hence it is interesting to see how the fraction of recirculating fluid changes with Grashof number. Fig. 7 shows the fraction of the cavity area containing contaminated fluid when the flow reaches its steady state, regardless of contaminant concentration. The parameter A_ψ/A_c is roughly a measure of the fraction of fluid recirculation in the cavity, where A_ψ represents the area of the recirculating flow (see insert in Fig. 7) and A_c presents the area of the cavity. It is observed that the fraction of the cavity area increases with the increase of Gr. With these conditions any contaminant left in the cavity following the start-up of the flow will only be further removed by the mixed convection.

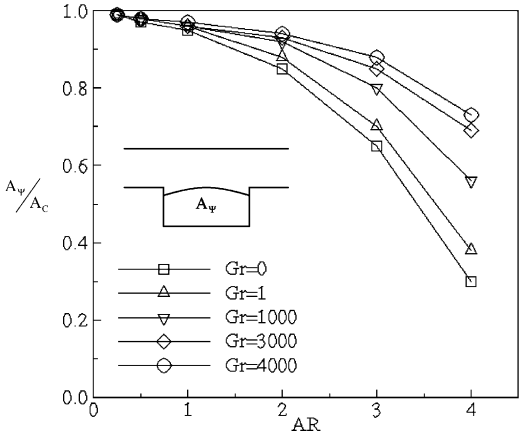

Fig. 7. Fraction of fluid trapped in cavities vs. cavity aspect ratio for varied Grashof numbers and $Re = 50$.

The previous work, Fang et al. [9] have shown that streamline patterns do not indicate how much of the contaminant is removed. To assess how fluid is purged from the cavity a number of fluid particles are introduced in the cavity, prior to initiating the flow. Initially 1600 markers are located in the cavity and Fig. 8(a)–(d) show the distribution of markers remaining in the cavity of AR = 4.0 with various Grashof numbers at steady state. It can be seen that more markers were removed from the cavity at large values of Gr and the distributions of markers in the cavities match the general distribution expected by observing the streamline patterns shown in Fig. 3. The percentage of markers removed as time progresses for various values of Gr as AR = 4 and $Re = 50$ is given in Fig. 9. The rate of removal of markers is high during the initial stages but becomes insignificant as time increases. For longer times the mixed convection dominates the removal process. Fig. 10 shows the percentage of markers (based on the total number of markers in the cavity before flow start-up)

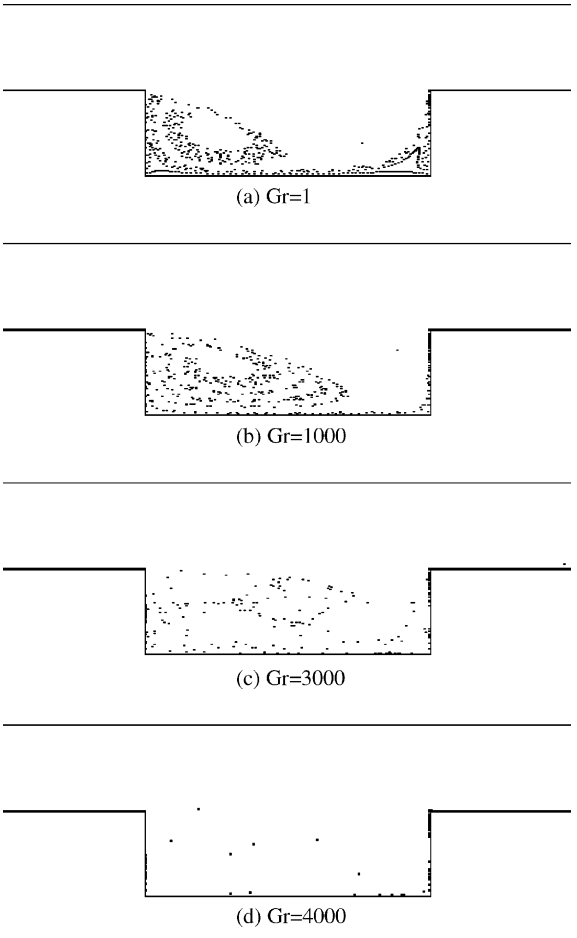

Fig. 8. Flow evolution of duct flow in a cavity of AR = 4 by using markers, for various Grashof numbers at $Re = 50$.

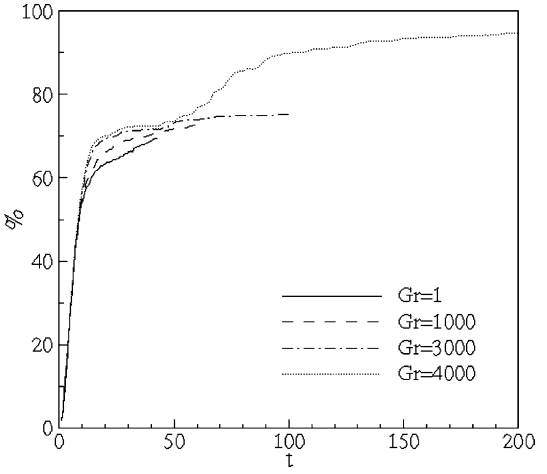

Fig. 9. Percentage of markers removed from the cavity vs. non-dimensional time for various Grashof numbers, at $Re = 50$ and AR = 4.0.

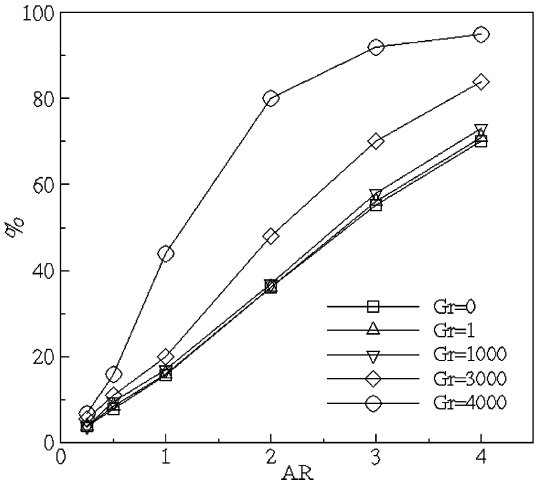

Fig. 10. Percentage of markers removed from the cavity for varied Grashof numbers at $Re = 50$.

removed from cavities for different values of Gr against AR. It can be seen that the percentage of markers removed from cavities increases with the increase of Gr. Within the scope of the present calculations a maximum of about 95% can be removed as AR = 4 and $Gr = 4000$.

The streamlines for the solutions at various values of Re while keeping Gr fixed at $Gr = 4000$ shown in Fig. 11. It is seen that the large central vortex has been stretched to fill the cavity as $Re = 100$. The outer flow penetrates a slight depth at the downstream end of the cavity. For the value of Re larger than 400, the central vortex shifts to the far right side of the cavity. For lower Reynolds number $Re \leqslant 100$, the isotherm in Fig. 12 shows that a large area of the cavity remains at higher temperature.

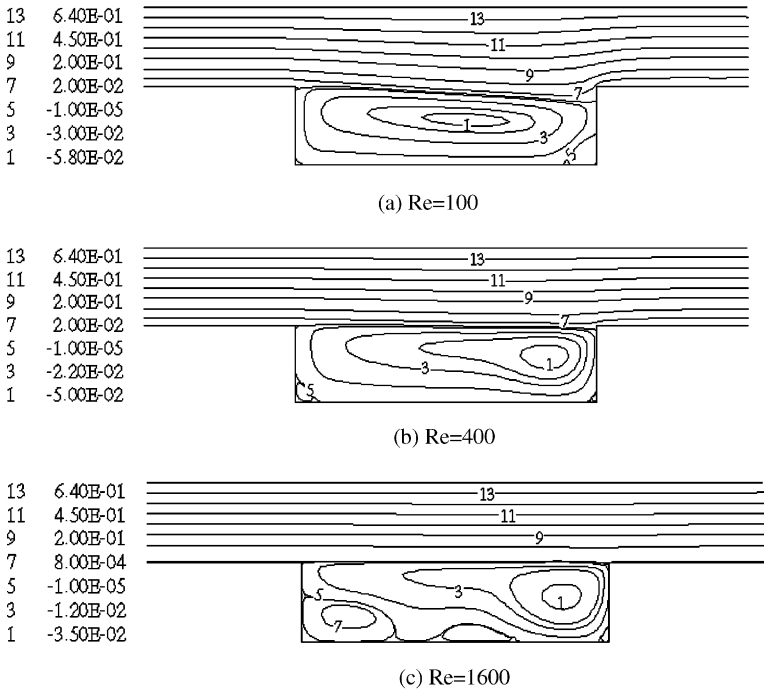

Fig. 11. Streamlines of duct flow over cavities with varied Reynolds numbers, $Gr = 4000$ and AR = 4 at steady state.

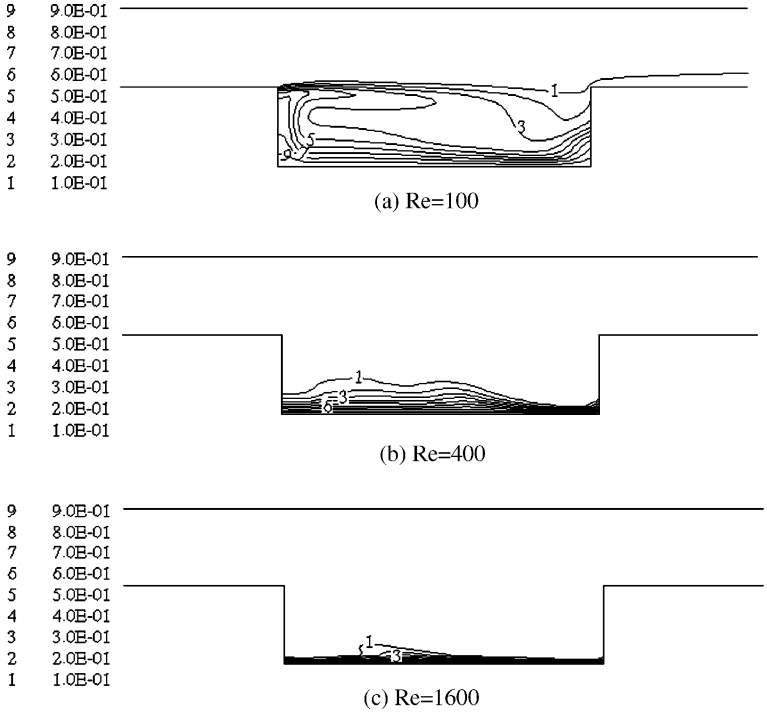

Fig. 12. Isotherms of duct flow over cavities with varied Reynolds numbers, $Gr = 4000$ and AR = 4 at steady state.

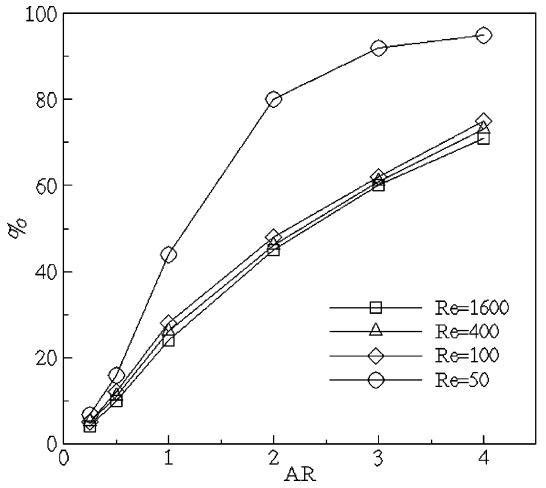

Fig. 13. Percentage of markers removed from the cavity for varied Reynolds numbers at $Gr = 4000$.

The area of low temperature increases with the increase of Reynolds number. It is reasonable that the buoyancy effect becomes insignificant while the region affected by the heat source becomes smaller due to the strong external flow. It is interesting to note that the removal of markers increases as Reynolds number decreases, shown in Fig. 13. These results are different from those without mixed convection in Fang et al. [9]. The main reason is that the strong buoyancy enhances the renewal process in the cavity at low Reynolds number. In addition, the effect of duct height H on cavity fluid removal as a function of cavity depth D is investigated in the present study. This means that the duct height is small compared to the cavity depth as the value of H/D decreases. Fig. 14 shows that the percentage of markers removed from a cavity increases with the increasing H/D.

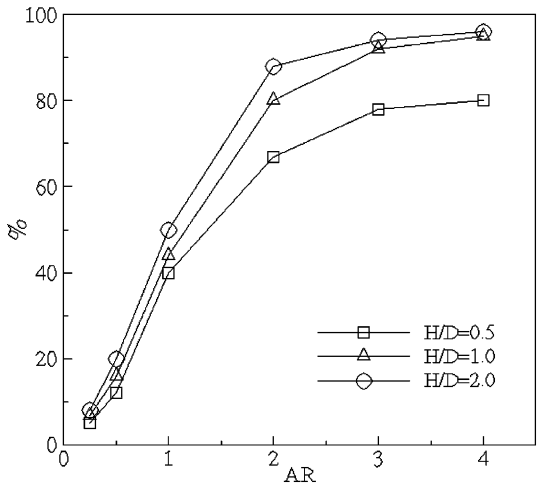

Fig. 14. Percentage of markers removed from the cavity for various values of H/D at $Gr = 4000$ and $Re = 50$.

4. Conclusions

Laminar flow solutions for duct flow over a rectangular cavity have illustrated the effect of mixed convection on the transient removal of contaminants contained in a cavity. The rate at which the contaminated cavity fluid is removed is relatively high during the unsteady start-up of the duct flow and approaches zero after the flow reaches a steady state. The results show that the change in Grashof number causes a dramatic difference in the observed flow patterns and cleaning efficiency. It can be seen that the cleaning process is enhanced as Grashof number is increased due to the interaction between the external duct flow and buoyancy-induced flow arising from a thermal source. It is interesting to note that for the values of Gr higher than 4000 the steady state result could not be obtained since oscillatory behavior was observed.

References

[1] J.L. Higdon, Stokes flow in an arbitrary two-dimensional domains: shear flow over ridges and cavities, J. Fluid Mech. 159 (1985) 195–226.
[2] U.B. Mehta, Z. Lavan, Flow in a two-dimensional channel with a rectangular cavity, Trans. ASME, J. Appl. Mech. 36 (1969) 897–901.
[3] V. O'Brien, Closed streamlines associated with channel flow over a cavity, Phys. Fluids 15 (1972) 2089–2097.
[4] I.S. Kang, H.N. Chang, The effect of turbulence promoters on mass transfer-numerical analysis and flow visualization, Int. J. Heat Mass Transfer 25 (1982) 1167–1181.
[5] H.N. Chang, H.W. Ryn, D.H. Park, Y.S. Park, Effect of external laminar channel flow on mass transfer in a cavity, Int. J. Heat Mass Transfer 30 (1987) 2137–2149.
[6] J.K. Alkire, D.B. Reiser, Effect of fluid flow on removal of dissolution products from small cavities, J. Electrochem. Soc. 131 (1984) 2795–2800.
[7] A. Yeckel, S. Middleman, L.A. Klumb, The removal of thin film from periodically grooved surfaces by an impinging jet, Chem. Eng. Commun. 96 (1990) 69–79.
[8] E.S. Mickaily, S. Middleman, M. Allen, Viscous flow over periodic surfaces, Chem. Eng. Commun. 117 (1992) 401–414.
[9] L.C. Fang, J.W. Cleaver, D. Nicolaou, Transient removal of a contaminated fluid from a cavity, Int. J. Heat Fluid Flow 20 (1999) 605–613.
[10] W.L. Oberkampf, L.I. Crow, Numerical study of the velocity and temperature fields in a flow-through reservoir ASME, J. Heat Transfer 98 (1976) 353–359.
[11] C.K. Cha, Y. Jaluria, Effect of thermal buoyancy on the recirculating flow in a solar pond for energy extraction and heat rejection ASME, J. Solar Energy Eng. 25 (1984) 428–437.
[12] E.M. Sparrow, F. Samie, Interaction between a stream which passes through an enclosure and nature convection

within the enclosure, Int. J. Heat Mass Transfer 25 (1982) 1489–1502.
[13] P.H. Oosthuizen, J.T. Paul, Mixed convection heat transfer in a cavity, in Fundamentals of Forced and Mixed Convection, ASME HTD 42 (1985) 159–169.
[14] E. Papanicolaou, Y. Jaluria, Mixed convection from an isolated heat source in a rectangular enclosure, Numer. Heat Transfer A 18 (1990) 427–461.
[15] F.H. Harlow, J.E. Welch, Numerical calculation of time-dependent viscous incompressible fluid with free surface, Phys. Fluids 8 (1965) 2182–2189.
[16] H. Miyata, S. Nishimura, Finite-difference simulation of nonlinear ship waves, J. Fluid Mech. 157 (1985) 327–357.
[17] A.J. Chorin, Numerical solution of the Navier–Stokes equations, Math. Comput. 22 (1968) 745–762.
[18] J.A. Viecelli, A computing method for incompressible flows bounded by moving walls, J. Comput. Phys. 8 (1971) 119–143.
[19] C.H. Kuo, M.A.R. Sharif, W.C. Scheriber, Numerical experiments on the simulation of Benard convection using marker and cell method, Chem. Eng. Commun. 127 (1994) 1–21.
[20] J.E. Welch, F.H. Harlow, J.P. Shannon, B.J. Daly, The MAC method—A computing technique for solving viscous, incompressible, transient fluid-flow problems involving a free surface, Los Alamos Scientific Lab. Rep. LA-3425, Los Alamos, 1966.